Microfluid Nanofluid (2013) 14:995–1010
DOI 10.1007/s10404-012-1107-3

RESEARCH PAPER

Phase diagrams of confined solutions of dimyristoylphosphatidylcholine (DMPC) lipid and cholesterol in nanotubes

Noriyoshi Arai · Kenji Yasuoka · Xiao Cheng Zeng

Received: 21 February 2012 / Accepted: 11 May 2012 / Published online: 20 December 2012

Abstract We have studied equilibrium morphologies of dimyristoylphosphatidylcholine lipid solution and cholesterol solution confined to nanotubes using dissipative particle dynamics (DPD) simulations. Phase diagrams regarding monomer concentration c versus radius of nanotube r for both solutions are attained. Three types of the inner surface of nanotubes, namely hydrophobic, hydrophilic, and hydroneutral are considered in the DPD simulations. A number of phases and molecular assemblies for the confined solutions are revealed, among others, such as the spiral wetting and bilayer helix. Several phases and assemblies have not been reported in the literature, and some are non-existence in bulk solutions. The ability to control the morphologies and self-assemblies within nanoscale confinement can be exploited for patterning interior surface of nanochannels for application in nanofluidics and nanomedical devices.

Keywords Self-assembly · Nanoscale confinement · Dissipative particle dynamics · Equilibrium morphology · Phase diagram

N. Arai (✉)
Department of Mechanical Engineering and Intelligent Systems, University of Electro-Communications, Tokyo 182-8585, Japan
e-mail: arai@mce.uec.ac.jp

K. Yasuoka
Department of Mechanical Engineering, Keio University, Yokohama 223-8522, Japan

X. C. Zeng
Department of Chemistry, University of Nebraska, Lincoln, NE 68588, USA

1 Introduction

Amphiphilic molecules such as surfactants and lipids are made up of two chemically distinctive functional groups, i.e., a hydrophilic head group and a hydrophobic tail group. As a result, these molecules can spontaneously assemble into a variety of microstructures and ordered morphologies, depending on, among other physical conditions, their chemical structures, concentration of molecules, and temperature (Israelachvili 1992; Gelbart et al. 1994). This "soft-matter polymorphism" for self-assembled morphologies not only has fundamental relevance to many biological processes, but also has been exploited in many industrial and domestic applications. The morphologies reported so far include spherical micelles, thread-like micelles, vesicles, membrane, and lamellar. Naturally, their physical properties hinge on organized assemblies in the solution (Shikata et al. 1987, 1989; Mathivet et al. 1996; Koubi et al. 2003; Rijcken et al. 2007; Arai et al. 2012). Nevertheless, it is still difficult to predict dynamical behavior and equilibrium morphologies of soft-matter due largely to the complexity of assembly structures.

It is also known that fluids confined to nanoscale channels can exhibit distinct phases not shown in the bulk (Rzayev and Hillmyer 2005; Meyer et al. 2006; Yoon et al. 2010; Lin et al. 2011). Some fluids such as water can show unusual dynamical behavior due to the nanoscale confinement. The water density close to the hydrophobic surface is lower than that in the bulk, and if a hydrophobic nanopore is sufficiently narrow, water within the nanopore can spontaneously evaporate (Lum et al. 1999; Powell et al. 2011). Strekalova et al. (2011) carried out Monte Carlo simulation of a water layer confined to a fixed and disordered matrix of hydrophobic nanoparticles. They revealed that even a small presence of hydrophobic nanoparticles

can drastically suppress thermodynamic fluctuations. In hydrophobic carbon nanotube or slit nanopore, the freezing transition of water may be either continuous or first order (Koga et al. 2001; Han et al. 2011). Also, water can freeze into various polymorphic phases of quasi-one-dimensional nanoice in carbon nanotubes (Maniwa et al. 2005; Bai et al. 2006).

When a solution of amphiphilic molecules is confined to a nanotube, equilibrium morphologies of the self-assembly of amphiphilic molecules are expected to be much richer due to more complex interactions involved with two chemically distinctive functional groups of the molecules. Not only the dimensional constraint imposed by the nanotube will affect the thermodynamic equilibrium, but also the chemical interactions among the nanotube, water, polar groups, and nonpolar groups will definitely disrupt the existing force balance in the bulk solution. In a previous DPD simulation study (Arai et al. 2008), we have shown variations of surfactant morphologies and polymorphic transitions for solutions (with short-chain surfactants) confined to nanotubes by changing chemical characteristics of the inner surface of nanotubes. This paper is an extension of the previous study. Here, more realistic and longer-chain molecules, namely dimyristoylphosphatidylcholine (DMPC) and cholesterol molecules are considered. A better understanding of the lipid and cholesterol morphologies on the molecular level will be of both fundamental and practical importance to biochemical and medical sciences.

Recently, several studies of DMPC lipid membrane and cholesterol systems have been reported (Khelashvili et al. 2010a, b; Cho et al. 2010). Cholesterol is known to be an essential component of cell membranes, and plays an important role in regulating properties of membranes. Doping a membrane with cholesterol can lead to more stable alignment. The aligned phase is typically formed at low temperatures and even at high lipid concentrations. Nyström et al. (2010) found that the lateral distribution of cholesterol in DMPC membrane is affected by transmembrane proteins. The latter can either decrease or increase the affinity of sterols for the lipid bilayers surrounding proteins. Shapiro et al. (2010) demonstrated the incorporation of cholesterol sulfate in DMPC bilayer systems. They found that cholesterol sulfate appeared to have combined features of both cholesterol and charged amphiphiles in the aligned phase. Meyer and Smit (2009) and Meyer et al. (2010) studied the effect of cholesterol of a phospholipid bilayer, as well as the DMPC-cholesterol phase diagram at different mol % of cholesterol and temperature, using molecular simulation.

In this work, we investigate equilibrium morphologies of DMPC lipid and cholesterol solutions confined to a nanotube by means of the DPD computer simulation. A main result of this study is the phase diagrams and associated morphologies of DMPC and cholesterol solutions with different monomer concentration c and at different radius of nanotube r.

2 Method and model

We employ the dissipative particle dynamics (DPD) (Hoogerbrugge and Koelman 1992; Groot and Warren 1997) method to simulate lipid molecule/water and cholesterol/water systems confined to different nanotubes, respectively. This method has been applied to various systems, including surfactant solutions (Arai et al. 2007; Angelikopoulos and Bock 2008; Can et al. 2009), membranes (Illya et al. 2006; Grafmueller et al. 2009; Li et al. 2009), molecular motors (Chen et al. 2007; Arai et al. 2010), etc. The DPD simulation allows relatively longer time and larger spatial scales required for simulating macromolecules or aggregations, because it describes motion of coarse-grained particles, each representing 10–20 atoms. Here, our DPD simulations typically require several microseconds to achieve thermodynamic equilibrium for each system. It is impractical to achieve this time scale on routine basis using atomistic molecular dynamics methods.

The motion of DPD particles obeys Newton's equations of motion,

$$m_i \frac{\mathrm{d}v_i}{\mathrm{d}t} = f_i = \sum_{j \neq i} F_{ij}^{\mathrm{C}} + \sum_{j \neq i} F_{ij}^{\mathrm{D}} + \sum_{j \neq i} F_{ij}^{\mathrm{R}} \tag{1}$$

where i is the particle index, m is the mass of a particle, v is the velocity, F_{ij}^{C} is a conservative force, F_{ij}^{R} is a pairwise random force, and F_{ij}^{D} is a dissipative force. The conservative force is normally a soft repulsion type and given by

$$F_{ij}^{\mathrm{C}} = \begin{cases} -a_{ij}\left(1 - \frac{|r_{ij}|}{r_{\mathrm{c}}}\right) n_{ij}, & |r_{ij}| \leq r_{\mathrm{c}} \\ 0, & |r_{ij}| > r_{\mathrm{c}} \end{cases}, \tag{2}$$

where a_{ij} is the parameter to determine magnitude of the repulsive force between particles i and j, r_{c} is a cutoff radius, $r_{ij} = r_j - r_i$, and $n_{ij} = r_{ij}/|r_{ij}|$. The random force and dissipative force are given by

$$F_{ij}^{\mathrm{R}} = \begin{cases} \sigma \omega^{\mathrm{R}}(|r_{ij}|)\zeta_{ij}\Delta t^{-1/2} n_{ij}, & |r_{ij}| \leq r_c \\ 0, & |r_{ij}| > r_c \end{cases} \tag{3}$$

and

$$F_{ij}^{\mathrm{D}} = \begin{cases} -\gamma \omega^{\mathrm{D}}(|r_{ij}|)(n_{ij} \cdot v_{ij}) n_{ij}, & |r_{ij}| \leq r_{\mathrm{c}} \\ 0, & |r_{ij}| > r_{\mathrm{c}} \end{cases} \tag{4}$$

respectively. Here σ is noise amplitude, γ is friction coefficient, ω^{R} and ω^{D} are r-dependent weight functions, $v_{ij} = v_j - v_i$ and ζ_{ij} is a random fluctuating variable with Gaussian statistics.

The random force and the dissipative force are linked by the "fluctuation–dissipation" theorem (Espanõl and Warren 1995), thereby one of the two weight functions appearing in Eqs. (3) and (4) can be chosen arbitrarily with a relation between the amplitude and k_BT,

$$\sigma^2 = 2\gamma k_B T \tag{5}$$

$$\omega^D(r) = \left[\omega^R(r)\right]^2 = \begin{cases} \left[1 - \frac{|r_{ij}|}{r_c}\right]^2, & |r_{ij}| \le r_c \\ 0, & |r_{ij}| > r_c \end{cases} \tag{6}$$

where k_B is the Boltzmann constant and T is temperature. Usually, reduced units are adopted for reporting the DPD results. The DPD unit of length is the cutoff radius, r_c, the unit of mass is the particle mass, m, and the unit of energy is k_BT.

In this study, following Meyer's approach (Meyer and Smit 2009; Meyer et al. 2010), we adopt a spring force with which the equilibrium bond distance is r_s and a bending force with which the equilibrium angle is θ_0 in the DMPC and cholesterol models. The spring force F^S_{ijk} and the bending force F^B_{ijk} are given by

$$F^S_{ij} = -k_{bond}\left(|r_{ij}| - r_s\right)n_{ij} \tag{7}$$

and

$$F^B_{ijk} = -\nabla\left(\frac{1}{2}k_{angle}\left(\theta_{ijk} - \theta_0\right)^2\right), \tag{8}$$

where k_{bond} is the spring constant and k_{angle} is the bending constant.

The DMPC model consists of eleven beads: three representing hydrophilic head groups (labeled by the letter h) and the other eight representing hydrophobic tail groups (labeled by the letter t). The cholesterol model consists of eight beads: one representing a hydrophilic group and the other seven representing hydrophobic groups. The nearest-neighbor beads in DMPC and in cholesterol are connected by a harmonic spring with a spring constant of 100, and the equilibrium bond length is 0.7. The bending force acts between consecutive bonds. In the DMPC lipid model, $k_{angle} = 6$ and $\theta_0 = 180°$ for the bonds between consecutive tail beads, and $k_{angle} = 3$ and $\theta_0 = 90°$ for the bonds between the head group connected to the tails or the first bead in both tails are used. On the other hand, $k_{angle} = 6$ and $\theta_0 = 180°$ for the bonds between consecutive tail beads is also used in cholesterol model. Moreover, it is known that cholesterol molecule has a stiff steroid ring structure. To capture this feature, we set the magnitude of the potential much larger than that of DMPC. These values are $k_{angle} = 100$ and $\theta_0 = 60°, 150°$. The units of k_{bond} and k_{angle} are k_B/r_c^2 and k_B/rad^2, respectively. The water particle (or monomer) is labeled by the letter w.

The interactions between any two particles in the solution are described by $a_{hw} = 15\ k_BT, a_{ww} = a_{tt} = 25\, k_BT$, $a_{hh} = 35\ k_BT$, and $a_{ht} = a_{tw} = 80\ k_BT$. This model assumes that the hydrophobic mismatch between the cholesterol and the DMPC hydrophobic tails is an important parameter regulating the cholesterol–lipid interactions. Relative lengths of hydrophilic and hydrophobic sections in the cholesterol molecule are properly described in this model.

The inner surface (or wall) of cylindrical nanotube is treated as a smooth surface. The potential function of the smooth wall is derived based on a structured wall by summing the DPD force between a particle and wall particles (Maddox and Gubbins 1997). Integration of this summed force results in a force between a particle and the smooth wall (within the cutoff distance r_c), i.e.,

$$F(R)^{wall} = \frac{1}{6}\pi\rho_{wall}a_{wall,p}\left(-R^4 + 2R^3 - 2R + 1\right)R/R, \tag{9}$$

where ρ_{wall} is the number density of the structured wall, $a_{wall,p}$ is the interaction parameter between the wall and a particle, $\boldsymbol{R}$ is the normal vector from the wall to the particle, and $R = |R|$ is the distance between the wall and the particle. Note that the wall-particle interaction is set to be independent of the curvature of the nanotube. The density of the wall particles ρ_{wall} is chosen to be 3.0, the same as the density of surfactant solution.

Here, the radius of nanotube is changed from 3.0 to 7.0 (in step of 1.0) in the dimensionless unit, and the total number of particles is varied from 4,239 to 23,079, depending on the radius of nanotube. The particle density ρ is 3, and the volume of the simulation box is $20 \times 20 \times 50$ in the dimensionless unit. The noise parameter is set at 3.0 and the friction parameter is set at 4.5. The initial configuration for the simulation is random, and the periodic boundary condition is applied in the axial direction of nanotube.

We have considered three kinds of nanotubes with distinct chemical interaction between water and the nanotube, namely, hydrophobic, hydrophilic, and hydroneutral. The interaction parameters, which can be viewed as a measure of the magnitude of surface energy, between hydrophobic wall and a water $a_{wall,w}$, and between the wall and the head group particle $a_{wall,h}$ are 70 k_BT, and that between the wall and the tail group $a_{wall,t}$ is 25 k_BT. In the case of hydrophilic nanotube, the interaction parameters $a_{wall,w}$ and $a_{wall,h}$ are 25 k_BT and $a_{wall,t}$ is 70 k_BT. In the case of hydroneutral nanotube, all three interaction parameters are 50 k_BT. These values of interaction parameters were used in our previous simulations (Arai et al. 2008). Note that hydrophilic and hydrophobic interactions are related to the solubility parameters. Values for various molecules have been examined by several research groups (Ryjkina et al. 2002; Shillcock and Lipowsky 2002, 2005; Nakamura and Tamura 2005; Yamamoto and Hyodo 2005; Özen et al. 2006; Illya et al. 2006). According to these previous

studies, favorable interactions (i.e., hydrophobic wall-tail, hydrophilic wall-head, and hydrophilic wall-water) can be represented by good solvent, e.g., they entail about same strength as head–head and tail–tail in dioleoylphosphatidylcholin (DOPC) molecule. In contrast, unfavorable interactions (i.e., hydrophobic wall-water, hydrophobic wall-head, and hydrophilic wall-tail) can be represented by poor solvent, e.g., they entail about same strength as water–tail group in cetyltrimethylammonium bromide (CTAB) molecule. Interactions between hydroneutral and all types of particle neither favor water nor tail or headgroups. The strength of interaction is similar to that of interaction between water and tail group of DOPC or hexaethylene glycol dodecyl ether (C12E6).

3 Results and discussions

3.1 Bulk morphology for DMPC and cholesterol solutions

Firstly, we perform simulations to investigate bulk morphologies of DMPC/water and cholesterol/water solutions. The total number of particles in the system is 81,000, and the density of solution is 3.0. Periodic boundary conditions are applied in all three spatial conditions. The concentration of lipid or cholesterol is changed from 10 to 100 %. Figure 1 shows representative snapshots of equilibrium morphologies of the DMPC lipid bulk solutions (a)–(d) and the cholesterol bulk solutions (e)–(h).

At very low concentration c, DMPC molecules assemble into spherical micelles and ellipsoidal micelles. At $c \approx 8.5$ %, a relatively large vesicle composed of a thousand DMPC molecules is formed (Fig. 1a). As c increases to ≈ 15 %, a lipid membrane is formed (Fig. 1b). The membrane stems from an opened vesicle which becomes more stable than closed vesicle as c increases. With further increasing c, the membrane begins to ripple, and then other membranes and thread-like micelles are formed in the simulation box. Hence, the phase at medium concentration exhibits a complex network structure. At $c \approx 70$ %, several membranes are regularly arranged in the simulation box, and the lamellar structure is formed as shown in Fig. 1c. Eventually, the lamellar phase transforms into the hexagonal lattice phase (Fig. 1d) with further increasing c. In normal hexagonal phases, the hydrophobic chains are contained within the cylindrical aggregates. However, because the DMPC molecule has more hydrophobic groups than hydrophilic ones, inverse hexagonal phase is formed with hydrophilic head within the cylindrical aggregates and

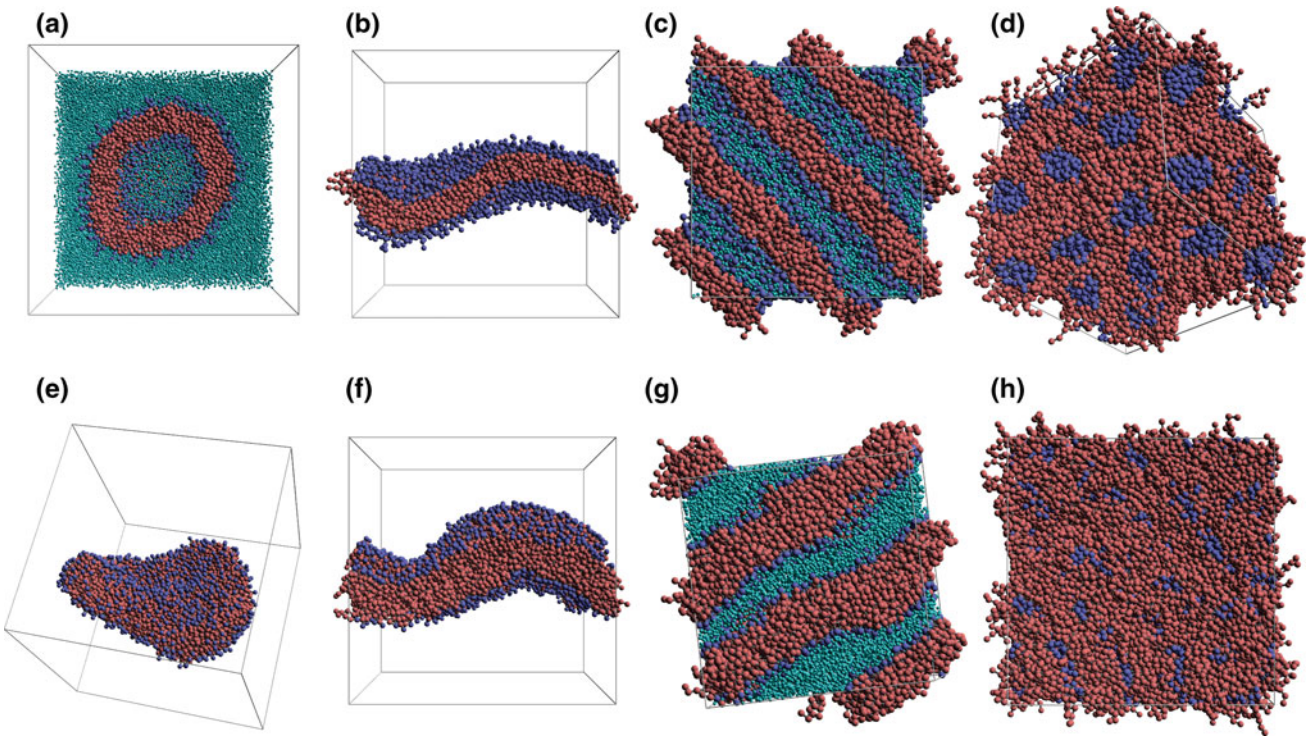

Fig. 1 Representative snapshots of equilibrium morphologies of DMPC lipid solutions (**a**–**d**) and the cholesterol solution (**e**–**h**). **a** A vesicle at $c = 8.5$ % (a *cross-sectional* view through the center of vesicle), **b** a bilayer at $c = 15$ %, **c** a lamellar at $c = 70$ %, **d** hexagonal morphology at $c = 100$ %; **e** a discoid micelle at $c = 10$ %, **f** a bilayer at $c = 20$ %, **g** a lamellar at $c = 60$ %, and **h** disordered and phase-separated morphology at $c = 100$ %. *Color code* water molecules in *aqua*, the head groups in *blue*, and the tail groups in *red*. Water particles are excluded in **b**, **e**, and **f** (color figure online)

the hydrocarbon chains fill the voids between the hexagonally packed cylinders.

On the other hand, in cholesterol solution, spherical and rod-like micelles emerge first at very low concentration. Next, a discoid micelle (Fig. 1e) and thick membrane (Fig. 1f) are formed at $c \approx 10$ and ≈ 20 %, respectively. The cholesterol molecule is stiffer than DMPC molecule, thus aggregates of cholesterol have low curvature. At relatively higher concentration ($c \approx 60$ %), the lamellar phase is segregated as in the case of DMPC solution (Fig. 1g). When c is higher than 90 %, the lamellar structure falls into disordered structure as shown in Fig. 1h. Hydrophilic domains are formed via head–tail separation, and these domains are entangled in this phase.

We estimate the end-to-end distance for the DMPC molecule and the cholesterol molecule as an equilibrium length of the molecule at different concentration. We define the end-to-end vector of the DPMC molecule as the line between terminal head particle and terminal tail particle; two end-to-end vectors are defined in a DMPC molecule, and the end-to-end vector of the cholesterol as the line between a head particle and terminal tail particle. As a result, the distribution of the equilibrium length of a DMPC or a cholesterol is almost the same at different concentration. The equilibrium length of a DMPC molecule (L_d) ~ 4.8, and that of a cholesterol molecule (L_c) ~ 4.2.

3.2 Morphologies of confined DMPC solution inside nanotube

3.2.1 *Hydrophobic nanotube*

In the first series of DPD simulations, we study phase behavior of DMPC lipid solutions confined to hydrophobic nanotubes. In Fig. 2, we show a phase diagram of the system and representative snapshots of equilibrium morphologies.

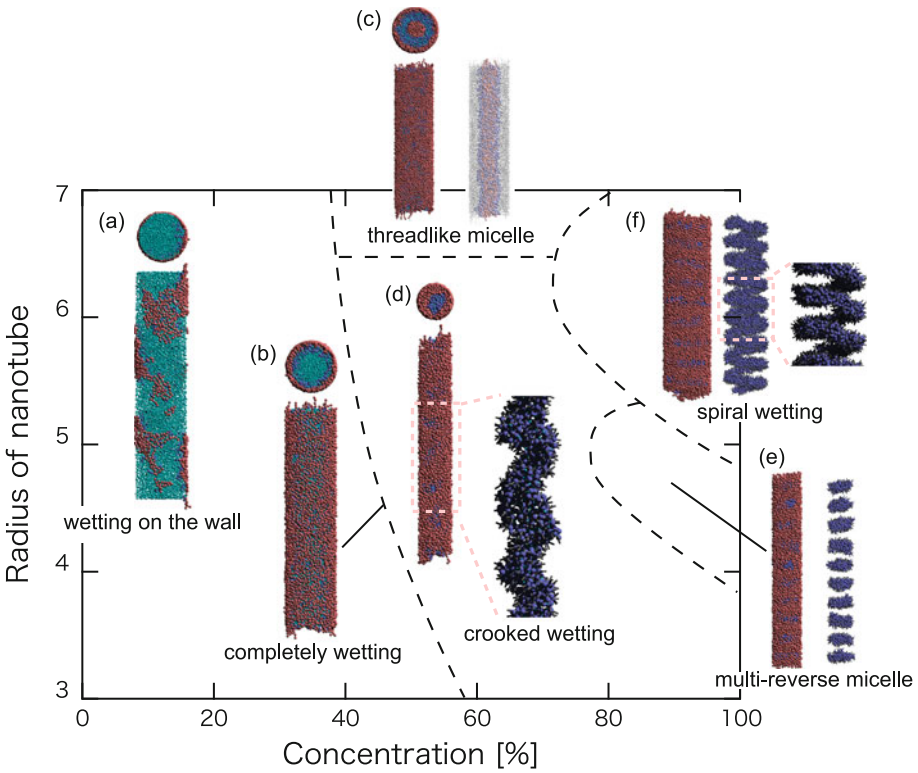

Fig. 2 A schematic phase diagram for the DMPC solution confined to hydrophobic nanotubes. The *vertical axis* is the radius of nanotube, and the *horizontal axis* is the concentration of the DMPC particles (or monomers). **a–f** Representative snapshots of equilibrium morphologies of the DMPC solution (nanotube not shown in the figure). **a** Wetting on the inner surface: *top panel* is the *top* view in axial direction, and *bottom panel* is a *side* view for $r = 6$ and $c = 10$ %. **b** Completely wetting on the wall: *top panel* is the *top* view in axial direction, and *bottom panel* is a *side* view for $r = 6$ and $c = 40$ %. **c** Thread-like micelle with a thin water layer: *top panel* is the *top* view in axial direction, *bottom left panel* is a *side* view; in *bottom right panel*, DMPC molecules (in *gray*) in direct contact with the nanotube are plotted much smaller to allow a view into the interior DMPC molecules and their morphologies for $r = 7$ and $c = 60$ %. **d** Crooked wetting on the wall: *top panel* is the *top* view in axial direction, *bottom left panel* is a *side* view, and *bottom right panel* is an enlarged *side* view of part of the *bottom left panel* where water molecules and tail groups are excluded from the snapshot for $r = 4$ and $c = 90$ %. **e** Multi-reverse micelle: *left panel* is a *side* view, and *right panel* is a *side* view of the *left panel* with tail groups being excluded from the snapshot for $r = 4$ and $c = 100$ %. **f** Spiral wetting on the wall: *left panel* is a *side* view, *middle panel* is a *side* view of *left panel* with tail groups being excluded from the snapshot, and *right panel* is an enlarged *side* view of part of the *middle panel* for $r = 4$ and $c = 100$ %. *Color code* water molecules in *aqua*, the head groups in *blue*, and the tail groups in *red* (color figure online)

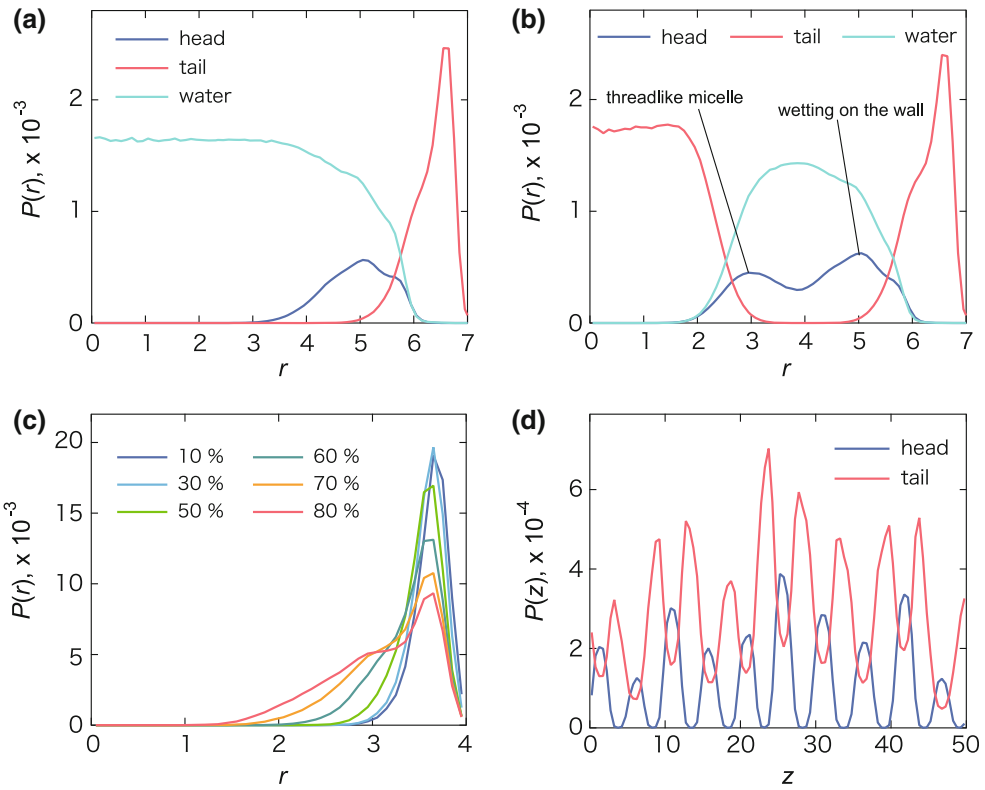

Fig. 3 Density profiles of head and tail groups and water of DMPC solutions confined to hydrophobic nanotubes. **a** Density profiles in the radial direction in the case of wetting on the wall in $r = 7$ and $c = 40$ %. **b** Same as **a** but for $r = 7$ and $c = 60$ %. **c** Concentration dependent of tail particle density profile in the radial direction for $r = 4$ and $c = 10$–80 %. **d** Head and tail particle density profile of the multi-reverse micelle in the axial direction for $r = 4$ and $c = 100$ %

The vertical axis of the phase diagram is the radius of nanotube r and the horizontal axis is the concentration of the DMPC particles (or monomers) c. Density profiles of the DMPC solution at representative conditions are shown in Fig. 3.

As expected, the tail groups of the lipid tend to be in direct contact with the hydrophobic nanotube. In all nanotubes considered, when c is very low, all DMPC molecules are adsorbed onto the inner surface of nanotube with their tail groups in contact with the nanotube, and their head groups in contact with interior water. Figure 3a shows density profiles for $r = 7$ and at $c = 40$ %. Tail particles are located in the interfacial region ($r > 5$), and head particles are sandwiched between the tail region and the interior water ($3 < r < 6$). Area of adsorption grows as c increases until the DMPC molecules completely wet the inner surface of the nanotube at $c \approx 40$–60 % (Fig. 2b).

For $r \geq 7$ and $c \approx 40$ %, the micelle is formed in the interior region of the nanotube due to the relatively larger radius. The micelle grows in the axial direction with increasing c, and becomes a single-strand thread-like micelle at $c \approx 60$ % (Fig. 2). In the right panel of Fig. 2c, graphic scales for those DMPC molecules in direct contact with the nanotube are drastically reduced so that one could look into the nanotube and see morphologies of interior DMPC molecules. This thread-like micelle occupies the central region of the nanotube with a thin circular water layer sandwiched between the outer wetting layer and the inner thread-like micelle. Radius of this thread-like micelle is estimated based on the peak position of head particle density distribution shown in Fig. 3b, which is about 3.

On the other hand, in nanotubes with $r \leq 6$, when the surface of nanotube is completely covered by DMPC molecules, effective radius of the nanotube is less than 3 which would be the radius of thread-like micelle composed of DMPC molecules. Thus, the thread-like micelle cannot be formed in central region of the nanotube, unlike in the case of $r \geq 6.5$. Excessive DMPC molecules thicken the existing adsorption layers (Fig. 3c) which can fill up into the nanotube. The right panel in Fig. 2d displays an enlarged side view of the system with tail particles of the DMPC molecule excluded from the picture for clarity. At these concentrations, a central hydrophilic domain begins to crook.

In the range of $4 < r < 5$, the head domain is disrupted and separated apart into several reverse micelles (Fig. 2e) as c increases. Reverse micelles in the central region are located in nearly the same intervals along the axial direction, and multi-reverse micelle structure is formed. Figure 3d shows the density profiles of head and tail particles of the DMPC molecules. An aggregation number for each reverse micelle is different, i.e., polydisperse reverse micelles are observed at very high c and $r \approx L_d$.

Middle and right panels in Fig. 2f are a side view, with tail particles of the DMPC molecule being excluded from the picture, and an enlarged side view of part of the middle

panel for $r = 7$. For $r > 5$, the head domain and water are regularly packed into the nanotube at high c due to restricted volume. Finally, a spiral hydrophilic domain appears with their tail groups in contact with the nanotube (right panel in Fig. 2f).

3.2.2 *Hydrophilic nanotube*

In the second series of DPD simulations, hydrophilic nanotubes are considered. In Fig. 4, we show the r versus c phase diagram and representative snapshots of equilibrium morphologies. In the hydrophilic nanotubes, water particles are preferred to be near the inner surface of the nanotube, while the DMPC molecules can aggregate into a variety of assemblies such as micelle and bilayer in the central region. At very low c, spherical micelles can develop in the central region of the nanotubes regardless of r. However, the aggregation number cannot increase when the r is too small. As shown in left and middle panels of Fig. 4a, several micelles are formed in the nanotube, whose radius is comparable to r. The formation of the vesicle observed in bulk is not seen in the nanotube with a radius $r = 7$, the largest radius considered in this study. Based on the end-to-end distance of a DMPC molecule, at least a radius of $2L_d$ ($\sim$9.6) is required for the formation of the vesicle. As c increases, the micelles are connected with each other and grow in the axial direction as c increases (right panel in Fig. 4a). At $c \approx 30$–40 %, an infinite straight thread-like micelle appears in the central region of the nanotube, surrounded by a thin circular water layer as shown in Fig. 4b, which is similar to the case of hydrophobic nanotube with $r = 7$ and at $c = 60$ % (Fig. 2c).

For $r > 4$, additional DMPC molecules can penetrate into the thread-like micelle, which nucleate into a reverse micelle (Fig. 4c) in the range of $40\ \% < c < 70\ \%$. The larger the radius of a nanotube is, the lower c at which the nucleation of reverse micelle occurs. This is because a molecule can invade into central region of the thread-like micelle more easily when the radius of nanotube is large. With c being further increased, a cylindrical bilayer is formed (Fig. 4d). Figure 5a shows density profiles of head particles in the range of $30\ \% < c < 60\ \%$ for $r = 5$. At $c = 30$ and 40 %, $P(r)$ near the central region ($r < 1$) is almost zero. A broad peak in the $P(r)$ curve emerges at $r < 1$ and $c = 50$ %, representing the formation of a core of reverse micelle. At $c = 60$ %, the cylindrical bilayer is formed, and consequently, the height of the central peak is comparable with height of outer peak ($r \sim 4$).

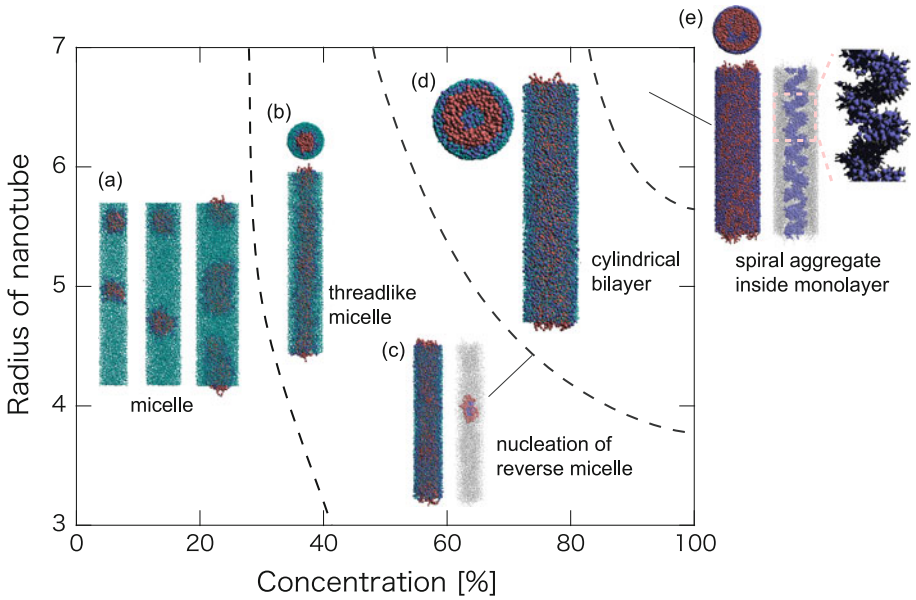

Fig. 4 A schematic phase diagram of DMPC solutions confined to hydrophilic nanotubes. The *vertical axis* is the radius of nanotube, and the *horizontal axis* is the concentration of the DMPC particles (or monomers). **a–e** Representative snapshots of equilibrium morphologies of DMPC solutions (nanotube not shown in the figure). **a** Micelles: the *left*, *middle*, and *right panels* are *side* views of a snapshot for $r = 4$ and $c = 10$ %, $r = 5$ and $c = 10$ %, and $r = 6$ and $c = 20$ %, respectively. **b** Thread-like micelle: *top panel* is the *top* view in axial direction, and *bottom panel* is a *side* view for $r = 5$ and $c = 30$ %. **c** Nucleation of reverse micelle: *left panel* is a *side* view; in *right panel* the DMPC molecules (in *gray*) in direct contact with the nanotube are plotted much smaller to allow a view into the interior DMPC molecules for $r = 5$ and $c = 60$ %. **d** Cylindrical bilayer: *left panel* is the *top* view in axial direction, *right panel* is a *side* view for $r = 6$ and $c = 60$ %. **e** Spiral wetting within monolayer: *top left panel* is the *top* view in axial direction, *bottom left panel* is a *side* view; in *middle panel* the DMPC molecules (in *gray*) in contact with the nanotube are plotted much smaller and interior tail groups are excluded to allow a view into the interior head group aggregate; *right panel* is an enlarged *side* view of part of the *middle panel* for $r = 7$ and $c = 100$ %. *Color code* water molecules in *aqua*, the head groups in *blue*, and the tail groups in *red* (color figure online)

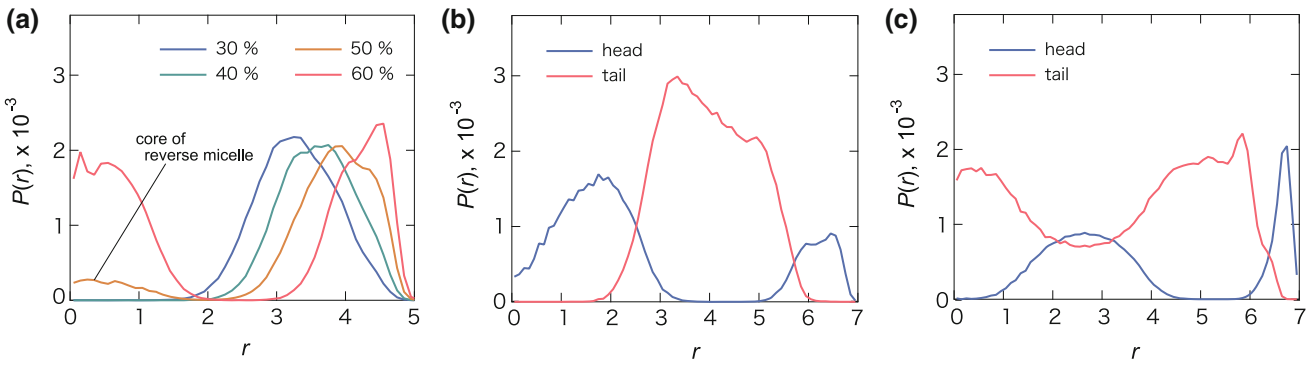

Fig. 5 Density profiles for DMPC solutions confined to hydrophilic nanotubes. **a** Concentration dependence of head particles density profiles in the radial direction for $r = 5$ and $c = 30$–60 %. Head and tail particle density profiles of **b** cylindrical bilayer and **c** in the case of spiral wetting within monolayer in the radial direction for $r = 7$ and $c = 70$ and 100 %, respectively

As c further increases, the cylindrical bilayer collapses and a hydrophilic domain begins to twist for $r \geq 6$. Lastly, the hydrophilic domain in the central region is in spiral structure and is also within a cylindrical monolayer with head groups in contact with the nanotube (Fig. 4e). Figure 5b, c shows that density profiles of head and tail particles for $r = 7$ and at $c = 70$ % (cylindrical bilayer) and 100 % (spiral aggregate inside monolayer), respectively. A peak in the density profile of tail particles in the case of cylindrical bilayer is located in $3 < r < 5$ for $c = 70$ % and it separates into two peaks for $c \approx 100$ %. Also, the peak in the density profile of head particles near $r \sim 7$ becomes sharper and the inner peak shifts slightly to outside ($r \sim 2.5$). The inner peak corresponds to the radius of spiral of central head particles.

3.2.3 *Hydroneutral nanotube*

In the third series, we investigate phase behavior of DMPC lipid solutions confined to hydroneutral nanotubes. In Fig. 6, we show the r versus c phase diagram and representative snapshots of equilibrium morphologies. The hydroneutral nanotubes neither favor water nor the tail or headgroups of the DMPC molecules. At very low c, DMPC lipids aggregate to semimicelles (Fig. 6a), and disk-shaped micelles are also formed when r is relatively small. In the semimicelles, the head groups of the amphiphilic molecule are in direct contact with water, while the tail groups are shielded from contacting with the water but in direct contact with the inner surface of the nanotube. In our previous simulation (Arai et al. 2008), we observed morphology of the coexisting spherical micelles with semimicelles in the hydroneutral nanotube at low concentrations because the radius of nanotube is larger than the size of molecule (surfactant). In the hydroneutral nanotube, the head groups always prefer to be in contact with water, while the water particles and the tail groups have the same chemical interaction parameter as the nanotube. Hence, if r is larger than the size of a molecule, the spherical micelles will develop in the central region, while the semimicelles will form on the wall. However, all DMPC lipid will be located near the nanotube when the size of molecule is large than the radius of nanotube r as in the present study. Therefore, semimicelles are exclusively formed in the present case.

As c increases, semimicelles are connected with each other to form partial thread-like micelles (Fig. 6a). It is known that the spherical end cap of the thread-like micelle is relatively unstable due to the lack of geometrically matching and packing parameter (Israelachvili 1992; Yang et al. 1997). A partial thread-like micelle relieves the energetic unstable configuration by directly contacting with the surface. For $r > 5$, all DMPC molecules gather together and an infinite-size aggregate, named as branched thread, is formed in the range of $40\ \% < c < 50\ \%$. The right panel in Fig. 6b shows a side view of the snapshot with water molecules being excluded for clarity. Thread-like micelles branch off in some places of the main aggregate, and they are in contact with the surface of nanotube like a partial thread.

For $c \approx 50$ %, all aggregates, including semimicelle, partial thread, and branched thread, transform into disks regardless of the radius of nanotube (Fig. 6c). For smaller r, highly ordered hybrid disk-like micelle is observed at lower concentrations, hence disks can be formed in the smaller aggregation number. In the hybrid-disk, head and tail particles are separated periodically in the axial direction, as clearly seen from both the snapshot and the density profiles shown in Fig. 7a1, a2. At very high concentrations ($c > 90$ %), disks are merged, and head and tail particles are separated in the radial direction as shown in Fig. 7b1, b2. So the assembly configuration depends delicately on r.

When $r \geq 6$, a central axis of hydrophilic domain is formed, and a hexagonal (Fig. 6d1) and a pentagonal (Fig. 6d2) phases emerge at $r = 7$ and 6, respectively. For

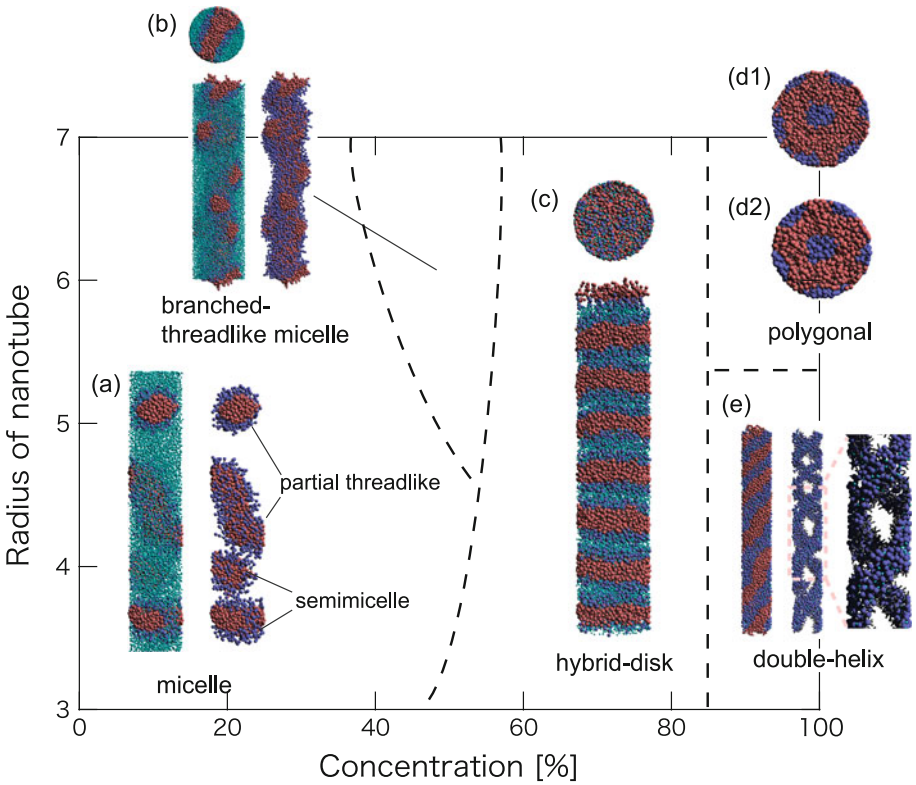

Fig. 6 A schematic phase diagram of DMPC solutions confined to hydroneutral nanotubes. The *vertical axis* is the radius of nanotube, and the *horizontal axis* is the concentration of the DMPC particles (or monomers). **a–e** Representative snapshots of equilibrium morphologies of DMPC solutions (nanotube not shown in the figure). **a** Semimicelle and partial threadlike micelle: *left panel* is a *side* view, and *right panel* is a *side* view with water particles being excluded for $r = 5$ and $c = 30$ %. **b** *Branched thread-like* micelle: *top left panel* is the *top* view in axial direction, *bottom left panel* is a *side* view, and *right panel* is a *side* view with water particles excluded for $r = 7$ and $c = 40$ %. **c** Hybrid disk: *top panel* is the *top* view in axial direction, and *bottom left panel* is a *side* view for $r = 6$ and $c = 60$ %. **d1**, **d2** Phase separation in polygonal pattern: *top panel* (*hexagonal pattern*) is the *top* view in axial direction for $r = 7$ and $c = 100$ %, and *bottom panel* (pentagonal pattern) is the *top* view in axial direction for $r = 6$ and $c = 100$ %. **e** Double-helix of head group domain: *left panel* is a *side* view, *middle panel* is a *side* view with tail groups excluded, and *right panel* is an enlarged *side* view of part of *middle panel* for $r = 4$ and $c = 90$ %. *Color code* water molecules in *aqua*, the head groups in *blue*, and the tail groups in *red* (color figure online)

$r = 4$, two threads composed of head groups of a lipid molecule twist along the surface of nanotube, and a double-helix structure is organized as shown in Fig. 6e.

3.3 Morphologies of confined cholesterol solution in nanotube

As compared with DMPC, cholesterol is a relatively stiff molecule due to the inclusion of phenanthrene in a molecule. Also, the length of a cholesterol molecule is shorter than DMPC lipid. Three series of simulations are also performed for which cholesterol solutions are confined to hydrophobic, hydrophilic and hydroneutral nanotubes, respectively.

3.3.1 Hydrophobic nanotube

In Fig. 8, we show the r versus c phase diagram and representative snapshots of equilibrium morphologies. As in the case of DMPC lipid in hydrophobic nanotube, the alkyl chain on the cholesterol tends to be in contact with the inner surface of the nanotube. At very low c, all cholesterol molecules wet the wall uniformly regardless of values of the radius (Fig. 8a). When c increases slightly, cholesterol nanodroplet is formed on the surface of nanotube. The formation of droplet occurs in some places of the wall of the nanotube at $c \approx 30$–40 %. The nanodroplet can grow on the wall in the circumferential direction. As a result, a circular droplet ring is generated.

Figures 8b and 9 show a snapshot of a cholesterol droplet for $r = 7$ at $c = 20$ % and concentration dependence of density profiles for tail particles in the range of $10\ \% < c < 50\ \%$. At $c \approx 10$ % (blue line), a sharp peak appears near the inner surface of nanotube. Toward the center of nanotube, $P(r)$ drastically decreases, and becomes almost zero at $r \sim 5$. The adsorption thickness is estimated to ~ 2. For $c > 20$ %, the peak located at $r \sim 6.5$ decreases and a second peak at $r \sim 6$ emerges with

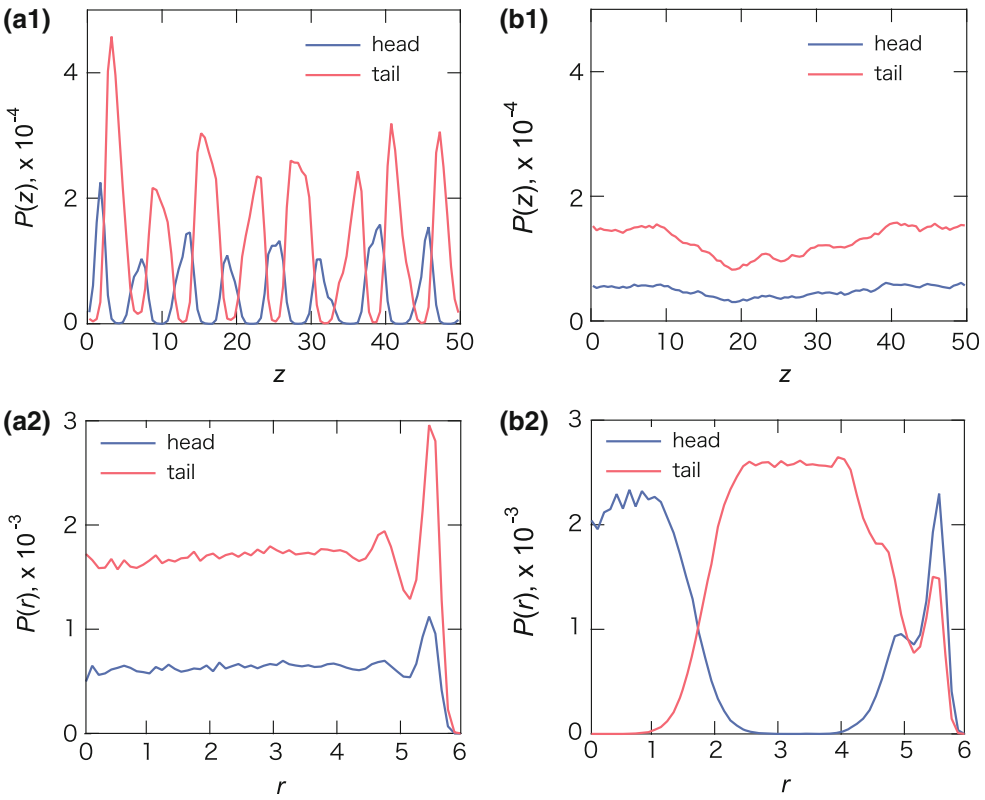

Fig. 7 Head and tail density profiles of DMPC solutions confined to hydroneutral nanotubes. **a1**, **a2** For $r = 6$ and $c = 80$ % in the axial and radial direction, respectively. **b1**, **b2** For $r = 6$ and $c = 100$ % in the axial and radial direction, respectively

increasing c. As r becomes smaller, $P(r)$ gradually decreases and becomes zero at $r \sim 3.5$. The latter value is nearly independent of c. Hence, the contact angle of droplet is almost a constant, independent of c.

At moderate concentrations, the entire surface of nanotube is covered by circular droplets and each circular droplet is periodically arranged in the axial direction (Figs. 8c, 9b). The right panel in Fig. 8c is an enlarged view of a cross section through the central axis of the nanotube for $r = 6$ at $c = 50$ %. It shows that an hourglass-like water nanochannel is formed due to circular droplets of the cholesterol. For $r \geq 6$, circular droplets coalesce together along the axial direction. A periodically spiral wetting on the wall occurs at $c \approx 70$ %. The left panel in Fig. 8d is an enlarged side view of with head particles being excluded for clarity, and it shows the formation of spiral water channel. As c further increases, the head domain is twisted off for $r \geq 6$ or if the hourglass structure is separated for $r < 6$. As a result, hourglass-disk coexisting phase is emerged at $c \approx 80$ %. Eventually, all aggregates transform into disks, and highly ordered hybrid disk-like micelle is formed at high concentrations (Fig. 8f1).

In contrast, when $r = 3$, the disk (columnar micelle) can be formed also at low concentrations because stable disk requires a small aggregation number. As c increases, the number of micelles increases. Lastly, hybrid-disk is formed, as in the case of larger radius of nanotube (Fig. 8f2).

3.3.2 Hydrophilic nanotube

In Fig. 10, we show the r versus c phase diagram and representative snapshots of equilibrium morphologies. At low c, cholesterol molecules aggregate into an ellipsoidal micelle. When r is relatively large, slightly-distorted micelle is formed due to relatively high stiffness of the molecules (left panel in Fig. 10a). When r is relatively small, a micelle is also formed with the head groups of cholesterol being in direct contact with the inner surface of nanotube because of the spatial confinement. As c increases, micelles are connected together and grow along the axial direction (right panel in Fig. 10a).

At $c \approx 40$–50 %, an infinite-size thread-like micelle is formed (Fig. 10b). Figures 10c and 11a display the top view of snapshots in the axial direction and the density profiles for head particles in the radial direction for $r = 3$ at $c = 50$, 70 and 100 %. The results reveal that the lateral radius of thread-like micelle becomes larger with increasing c when r is relatively small (≤ 4). In contrast, when r is relatively large (≥ 5), parts of thread-like micelle become thick at $c \approx 50$ %. Left and right panels in Fig. 10d show a side view of snapshots with water particles being excluded from the view, and an enlarged view of a cross section through the central axis of the nanotube for $r = 7$ at $c = 50$ %, respectively. We observe some head particles and water molecules within the thicker part of thread-like micelle, as well as a partially cylindrical bilayer.

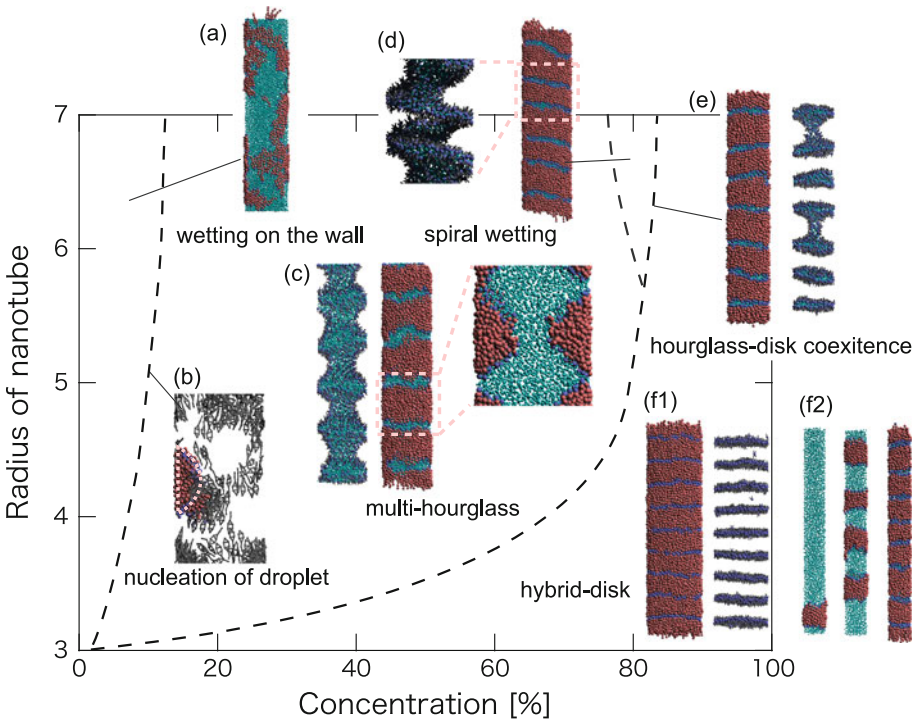

Fig. 8 A schematic phase diagram of cholesterol solutions confined to hydrophobic nanotubes. The *vertical axis* is the radius of nanotube, and the *horizontal axis* is the concentration of the cholesterol particles (or monomers). **a**–**f** Representative snapshots of equilibrium morphologies of cholesterol solutions (nanotube not shown in the figure). **a** Wetting on the wall: a *side* view for $r = 6$ and $c = 10$ %. **b** Nucleation of cholesterol droplet: an enlarged *side* view of one part of snapshot for $r = 7$ and $c = 20$ %, where cholesterol molecules not in the droplet are colored in *gray* for clarity. **c** Multi-hourglass: *middle panel* is a *side* view, *left panel* is a *side* view with tail groups excluded, and *right panel* is an enlarged *cross-sectional* view through the *central axis* of the nanotube for $r = 6$ and $c = 50$ %. **d** Spiral wetting on the wall: *right panel* is a *side* view, and *left panel* is an enlarged *side* view of part of the *right panel* with tail groups excluded for $r = 7$ and $c = 70$ %. **e** Hourglass-disk coexistence: *left panel* is a *side* view, and in *right panel* tail groups are excluded for $r = 5$ and $c = 80$ %. **f1**, **f2** Hybrid-disk: **f1** *left panel* is a *side* view, and in *right panel* tail groups are excluded for $r = 7$ and $c = 100$ %. **f2** *Left middle*, and *right panels* are *side* views for $r = 3$ and $c = 10$, 40, and 90 %, respectively. *Color code* water molecules in *aqua*, the head groups in *blue*, and the tail groups in *red* (color figure online)

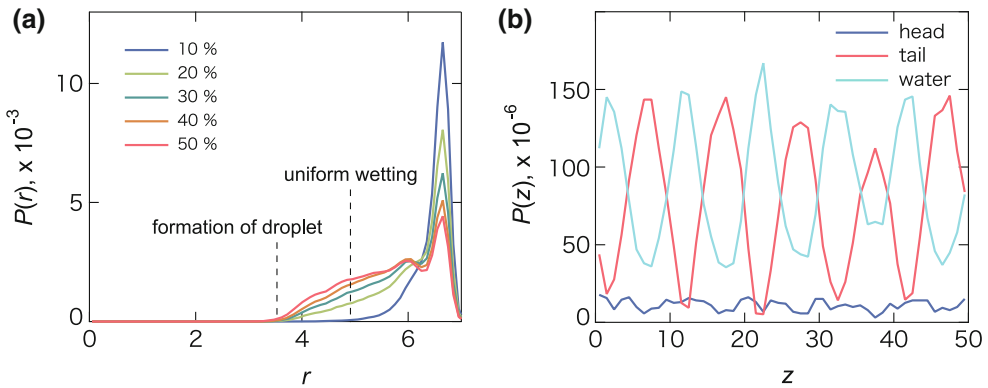

Fig. 9 Density profiles of cholesterol solutions confined to hydrophobic nanotubes. **a** Concentration dependence of tail particle density profiles in the radial direction for $r = 7$ and $c = 10$–50 %. *Vertical dashed lines* represent thickness of adsorption layer of cholesterol molecules for $c = 10$ %, and for $c = 20$–50 %, respectively. **b** Head, tail and water particle density profiles of the multi-hourglass in the axial direction for $r = 6$ and $c = 50$ %

As c further increases, the partially cylindrical bilayer grows in the axial direction. A full cylindrical bilayer is formed at $c \approx 50$–80 %, depending on r (Fig. 10e1). For $r = 7$, a water layer appears in the central region ($r < 1$) as shown in Figs. 10e2 and 11b. The morphology at high concentrations is dependent on the ratio between the radius

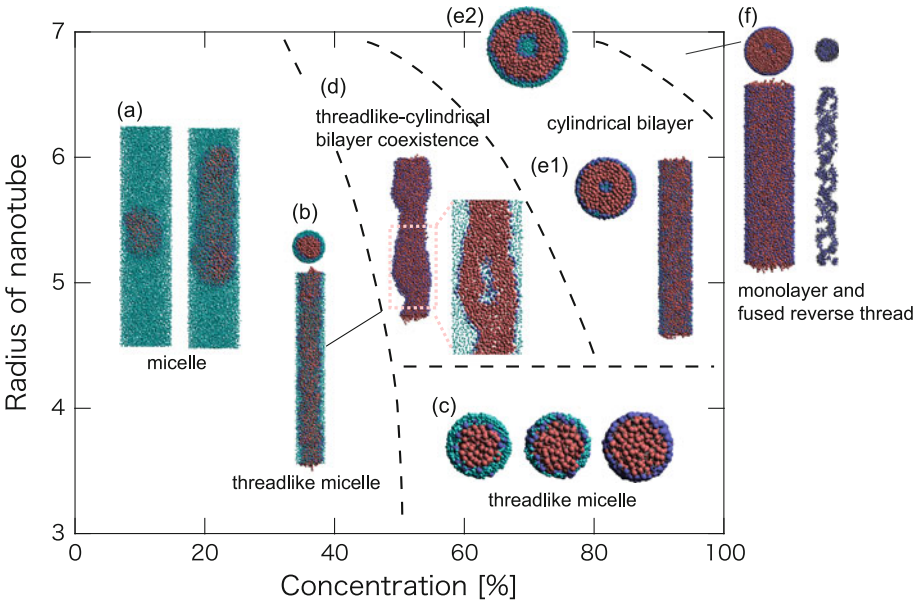

Fig. 10 A schematic phase diagram of cholesterol solutions confined to hydrophilic nanotubes. The *vertical axis* is the radius of nanotube, and the *horizontal axis* is the concentration of the cholesterol particles (or monomers). **a**–**f** Representative snapshots of equilibrium morphologies of cholesterol solutions (nanotube not shown in the figure). **a** Micelle: *left* and *right panels* are *side* views for $r = 6$ and $c = 10$, and 30 %. **b** Formation of percolated thread-like micelle: *top panel* is the *top* view in the axial direction, and *bottom panel* is a *side* view for $r = 4$ and $c = 50$ %. **c** Thread-like micelle: *left*, *middle* and *right panels* are *top* view in the axial direction for $r = 3$ and $c = 50$, 70, and 90 %, respectively. **d** Thread-like cylindrical bilayer coexistence: *left panel* is a *side* view with water particles excluded, and *right panel* is an enlarged *cross-sectional* view through the *central axis* of the nanotube for $r = 7$ and $c = 50$ %. **e1**, **e2** Cylindrical bilayer: **e1** *left panel* is the *top* view in the axial direction, and *right panel* is a *side* view for $r = 5$ and $c = 90$ %. **e2** *Top view* in the axial direction for $r = 7$ and $c = 70$ %. **f** Fused reverse thread inside monolayer: *top left panel* is the *top* view in the axial direction, *bottom left panel* is a *side* view, *top right panel* is the *top* view with tail particles and head particles in contact with the nanotube excluded in the axial direction, and *bottom right panel* is a *side* view for $r = 7$ and $c = 100$ %. *Color code* water molecules in *aqua*, the head groups in *blue*, and the tail groups in *red* (color figure online)

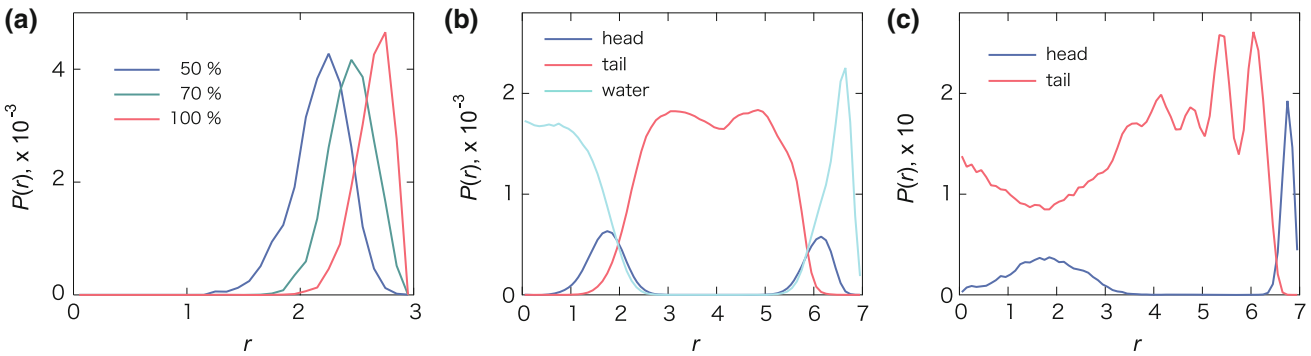

Fig. 11 Density profiles of cholesterol solutions confined to hydrophilic nanotubes. **a** Concentration dependence of head particles density profile in the radial direction for $r = 3$ and $c = 50$, 70 and 100 %. **b**, **c** Head, tail and water particle density profiles of cylindrical bilayer and fused reverse thread inside monolayer in the radial direction for $r = 7$ and $c = 70$ and 100 %, respectively

of the cylindrical bilayer and the radius of nanotube. For the present cholesterol model, the morphology is the cylindrical bilayer for $r \geq 5$, whereas the thread-like micelle is formed for $r < 5$ at high c.

Figures 10f and 11c show snapshots and density profiles of head and tail particles for $r = 7$ at $c = 100$ %, respectively. A cylindrical monolayer of head particles is observed near the inner surface of nanotube ($r > 6.5$). The right panels in Fig. 10f display a side view with the monolayer and hydrophobic tails being excluded from the view. At $c = 100$ %, the central water layer seen in Fig. 10e2 is no longer existence. The cholesterol molecules occupy the central region, where thread-like hydrophilic domains are entangled inside the monolayer.

3.3.3 Hydroneutral nanotube

Finally, we study phase behavior of cholesterol solutions confined to hydroneutral nanotubes. In Fig. 12, we show r versus c phase diagram and representative snapshots of equilibrium morphologies. At low c, cholesterol molecules form a variety of organized assemblies such as semimicelle, disk, and semivesicle (Fig. 12a1, a2), depending on the aggregation number and the radius of nanotube. Semivesicle is only observed for $r = 7$, and because it is in direct contact with the inner surface of nanotube, water molecules are as c increases, disk-shaped micelle is formed. There are a chipped disk (Fig. 12a3) or a tilted disk (Fig. 12a4) in the kind of typically the disk. In bulk solutions, randomly dispersed amphiphilic molecules aggregate into several isolated small micelles (core of micelle) in the early stage. In the late stage, the small micelles are connected together and grow into a large and stable assembly whose shape can be rod-like shape or thread-like, among others (Arai et al. 2007). In the nanotube with relatively small r, stable disk-shaped micelle is formed in the early stage since relatively small aggregation number is needed to form a disk. However, when the radius of nanotube is relatively large, larger aggregation numbers are needed to form a stable disk. Thus, core of micelles and semimicelles merge together to form a stable disk. If the aggregation number of merged micelle is slightly less than that of stable disk, the chipped disk is formed. Otherwise, a tilted disk is formed with larger aggregation number. Although it is not observed in this simulation, we expect that a ring-shaped micelle in the radial direction (Arai et al. 2008) can emerge, given a large number of the chipped micelle in a nanotube with a very large r.

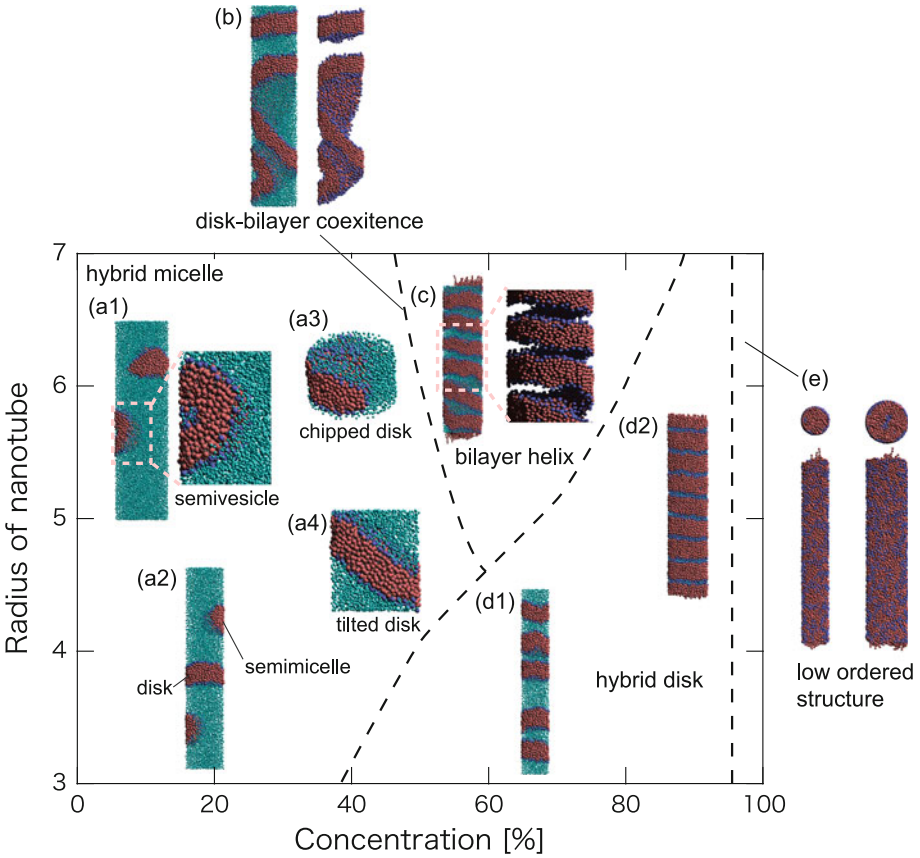

Fig. 12 A schematic phase diagram of cholesterol solutions confined to hydroneutral nanotubes. The *vertical axis* is the radius of nanotube, and the *horizontal axis* is the concentration of the cholesterol particles (or monomers). **a–f** Representative snapshots of equilibrium morphologies of the cholesterol solution (nanotube not shown in the figure). **a1–a4** Hybrid micelle: **a1** *left panel* is a *side* view, *right panel* is an enlarged *side* view of part of the *left panel* for $r = 7$ and $c = 10$ %. **a2** A *side* view for $r = 5$ and $c = 20$. **a3** A *side* view of the clipped part for $r = 7$ and $c = 30$ %. **a4** A *side* view of the clipped part for $r = 6$ and $c = 30$ %. **b** Disk-bilayer coexistence: *left panel* is a *side* view, and *right panel* is a *side* view with water particles excluded for $r = 6$ and $c = 50$ %. **c** Bilayer helix: *left panel* is a *side* view, and *right panel* is an enlarged *side* view of part of the *left panel* with water particles excluded for $r = 7$ and $c = 70$ %. **d1**, **d2** Hybrid-disk: *side* views for $r = 4$ and $c = 50$ % (**d1**) and $r = 6$ and $c = 90$ % (**d2**). **e** Disordered structure: *top left panel* is the *top* view in the axial direction, *bottom left panel* is a *side* view for $r = 4$ and $c = 100$ %. *Top right panel* is the *top* view in the axial direction, *bottom right panel* is a *side* view for $r = 6$ and $c = 100$ %. *Color code* water molecules in *aqua*, the head groups in *blue*, and the tail groups in *red* (color figure online)

For $r > 5$, several assemblies are combined into twisted bilayer with its edge being in direct contact with the wall at $c \approx 50$ % (Fig. 12b). Moreover, the twisted bilayer is straighten up as c increases, and eventually, a bilayer helix is formed at $c \approx 70$ % (Fig. 12c). The bilayer helix does not appear for $r < 4$, since $r < L_c$ for which the bilayer cannot have enough curvature to form the helix structure. Thus, in a nanotube with a relatively small r, all aggregates transform into a disk-like micelle at modest concentrations (e.g., $c \approx 40$ %) (Fig. 12d1). A highly ordered hybrid disk is formed at $c \approx 70$ %. In a nanotube with relatively large r, a hybrid disk is observed at $c \approx 80$ % (Fig. 12d2). Lastly, at $c \approx 100$ % and for all r's, the highly ordered hybrid disk is broken up and the cholesterol molecules form a disordered structure.

4 Discussions

When DMPC lipids or cholesterol solutions are confined to nanotubes, they can exhibit a sequence of "soft-matter polymorphic" transitions with increasing the molecular concentration. A DMPC lipid molecule is similar to a cholesterol molecule in the molecular length and chemical interactions between the molecular and a solvent (water) and the wall of nanotubes. Hence, the sequence of transitions in bulk DMPC solutions is similar to those of cholesterol solutions, which include the spherical micelle and the thread-like micelle at low concentrations, the bilayer membrane at medium concentrations, and the lamellar micelle at high concentrations. It is mentioned in our early work (Arai et al. 2008) that the sequence of transitions in the hydrophilic nanotube is similar to that in the bulk, because the hydrophilic nanotube somewhat mimics the water environment surrounding the solute molecules as long as the chemical interaction with the solute is concerned. Indeed, we confirm that the sequence to transitions in hydrophilic nanotube is similar to those in the bulk. Note that although the cylindrical lamellar phase, which corresponds to the lamellar phase in bulk, did not appear at high concentrations in this simulation, this phase is expected to form in larger radius of nanotube. Hence, the new morphologies observed inside the hydrophilic nanotubes such as spiral aggregate inside monolayer and those shown in Fig. 4e should be attributed to the effect of confinement.

On the other hand, there are differences between the DMPC lipid and cholesterol molecule. A DMPC molecule has two hydrophobic chains, which means that the volume of hydrocarbon chain in the assemblies is larger than that of cholesterol. In addition, a cholesterol molecule has a phenanthrene part, and is more stiff compared to a DMPC molecule. Due to their differences in molecules, equilibrium morphologies and self-assembly process differ as well. The morphologies of DMPC solutions in hydrophobic nanotubes at very low concentrations closely resemble those of cholesterol solutions. However, at the moderate and high concentrations, their morphologies can be greatly affected by the chemical nature of molecules. For a DMPC lipid, a single straight or crooked thread-like micelle is formed within a wetting monolayer at moderate concentrations, and a spiral wetting phase at high concentrations. This sequence of morphology transitions is in analogous with those in hydrophobic nanotubes. In addition, we estimated the cross-section density for each nanotube. These densities were almost constant in all ranges except near wall. Therefore, the hydrophobic nanotubes may be viewed as hydrophilic nanotubes with a smaller radius, where the head groups of the wetting monolayer are all pointing inward towards the central axis. However, the multi-reverse micelle phase as shown in Fig. 2e is not seen in the hydrophilic nanotubes. This phase possesses a delicate structure if the radius of nanotubes is approximately the same as the molecular length.

However, the cholesterol solutions confined to the hydrophobic nanotubes show different morphologies compared to the hydrophilic nanotubes. The hourglass-like aggregate or the spiral wetting phase is formed at moderate concentrations, and the highly ordered hybrid disk is resulted at high concentrations. For relative small r or at high concentrations, the cholesterol solutions tend to orient in the axial direction of nanotubes due to the molecular stiffness. Thus, one can view the hybrid-disk at very high concentration as a smectic liquid crystal phase in one dimension. Since tail groups in cholesterol are in direct contact with the inner surface of the nanotube, those aggregates that are connected in the axial direction such as a thread-like micelle cannot be formed. However, the hourglass and disk, which are developed in the radial or circumferential direction, are formed and packed in the axial direction.

In hydroneutral nanotubes, various unique assemblies appear, such as a semivesicle and a partial thread-like micelle; also the semimicelle as a minimum unit in both molecules appears at low concentrations. As c increases, cholesterol molecules fill up the nanotubes so that a molecule does not bend, as in the case of hydrophobic nanotubes, so that the disk-like micelle and twisted bilayer are formed at moderate concentrations. On the other hand, the DMPC lipid, which is a soft molecule compared to cholesterol, aggregates into a branched thread-like micelle via growing partial threads. Since chemical nature of the wall is hydroneutral, i.e., neither favors water nor the head or tail groups, DMPC molecules tend to orient in the axial direction. As a result, the hybrid-disk phase appears in both molecules at high concentrations. It also seems that the disk surface composed of DMPC molecules jumbles. At very high concentrations, a highly ordered axial structure,

the hybrid disk, is broken up, and transforms into other hybrid forms (but not in axial direction). This indicates that water molecules play an important role to orient cholesterols in the axial direction.

5 Conclusion

In this study, phase behavior of DMPC and cholesterol solutions confined to different nanotubes is simulated as a function of the monomer concentration and the radius of nanotubes. Morphologies and polymorphic transitions are investigated as the chemical characteristics of the inner surface of nanotubes and the radius of nanotubes are changed. For morphologies, the larger radius of the nanotubes, the more diversified phases are formed, such as a spiral wetting phase and a bilayer helix phase. These phases are observed for $r > 4$ or 5, even though the equilibrium length of a molecule L is larger than the radius of nanotubes r. Molecules are packed parallel to the axial direction of nanotubes when r is relatively small. Thus, few degrees of freedom of assembly configurations are resulted. In contrast, a variety of assembles can be formed for larger r, because the solute molecules can tilt in the radial direction. Indeed, more diverse equilibrium morphologies will be generated if r is larger than L. This finding indicates that the ratio L to r is one of the important parameters that can influence morphologies of the system confined to a nanotube. However, in all types of nanotubes, the larger r is required for morphology diversification of cholesterol than that of DMPC, regardless of $L_d > L_c$. We also find that morphologies confined to a nanotube are strongly affected by the molecular stiffness. Our simulations offer a guide to control morphologies of assemblies in nanoscale confinement, with potential applications in nanofluidic devices.

Acknowledgments N.A. and K.Y. were supported by the Core Research for Evolution Science and Technology (CREST) of the Japan Science and Technology Corporation (JST). XCZ was supported by grants from the NSF (CBET-1036171 and CBET-1066947) and ARL (W911NF1020099).

References

Angelikopoulos P, Bock H (2008) Directed self-assembly of surfactants in carbon nanotube materials. J Phys Chem B 112(44): 13793–13801

Arai N, Yasuoka K, Masubuchi Y (2007) Spontaneous self-assembly process for threadlike micelles. J Chem Phys 126(24):244905

Arai N, Yasuoka K, Zeng XC (2008) Self-assembly of surfactants and polymorphic transition in nanotubes. J Am Chem Soc 130(25): 7916–7920

Arai N, Yasuoka K, Koishi T, Ebisuzaki T (2010) Asymmetric Brownian motor driven by bubble formation in a hydrophobic channel. ACS Nano 4(10):5905–5913

Arai N, Yasuoka K, Zeng XC (2012) Nanochannel with uniform and Janus surfaces: shear thinning and thickening in surfactant solution. Langmuir 28(5):2866–2872

Bai J, Wang J, Zeng XC (2006) Multiwalled ice helixes and ice nanotubes. Proc Natl Acad Sci USA 103(52):19664–19667

Can H, Kacar G, Atilgan C (2009) Surfactant formation efficiency of fluorocarbon- hydrocarbon oligomers in supercritical CO(2). J Chem Phys 131(12):124701

Chen Q, Li DY, Oiwa K (2007) The coordination of protein motors and the kinetic behavior of microtubule—a computational study. Biophys Chem 129(1):60–69

Cho HS, Dominick JL, Spence MM (2010) Lipid domains in bicelles containing unsaturated lipids and cholesterol. J Phys Chem B 114(28):9238–9245

Espanõl P, Warren PB (1995) Statical-mechanics of dissipative particle dynamics. Europhys Lett 30(4):191–196

Gelbart WM, Ben-Shaul A, Roux D (1994) Micelles, membranes, microemulsions, and monolayers. Springer, New York

Grafmueller A, Shillcock JC, Lipowsky R (2009) The fusion of membranes and vesicles: pathway and energy barriers from dissipative particle dynamics. Biophys J 96(7):2658–2675

Groot RD, Warren PB (1997) Dissipative particle dynamics: bridging the gap between atomistic and mesoscopic simulation. J Chem Phys 107(11):4423–4435

Han S, Choi MY, Cumar P, Stanley HE (2011) Phase transitions in confined water nanofilms. Nat Phys 6(9):685–689

Hoogerbrugge PJ, Koelman JMVA (1992) Simulating microscopic hydrodynamic phenomena with dissipative particle dynamics. Europhys Lett 19(3):155–160

Illya A, Lipowsky R, Shillcock JC (2006) Two-component membrane material properties and domain formation from dissipative particle dynamics. J Chem Phys 125(11):114710

Israelachvili JN (1992) Intermolecular and surface forces. Academic Press, London

Khelashvili G, Pabst G, Harries D (2010a) Cholesterol orientation and tilt modulus in DMPC bilayers. J Phys Chem B 114(22):7524–7534

Khelashvili G, Mondal S, Andersen OS, Weinstein H (2010b) Cholesterol modulates the membrane effects and spatial organization of membrane-penetrating ligands for G-protein coupled receptors. J Phys Chem B 114(37):12046–12057

Koga K, Gao G, Tanaka H, Zeng XC (2001) Formation of ordered ice nanotubes inside carbon nanotubes. Nature 412(6849):802–805

Koubi L, Salz L, Tarek M, Scharf D, Klein ML (2003) Influence of anesthetic and non- immobilizer molecules on the physical properties of a polyunsaturated lipid bilayer. J Phys Chem B 107(51):14500–14508

Li XJ, Pivkin IV, Liang HJ, Karniadakis GE (2009) Shape transformations of membrane vesicles from amphiphilic triblock copolymers: a dissipative particle dynamics simulation study. Macromolecules 42(8):3195–3200

Lin S, Shih CJ, Strano MS, Blankschtein D (2011) Molecular insights into the surface morphology, layering structure, and aggregation kinetics of surfactant-stabilized graphene dispersions. J Am Chem Soc 133(32):12810–12823

Lum K, Chandler D, Weeks JD (1999) Hydrophobicity at small and large length scales. J Phys Chem B 103(22):4570–4577

Maddox MW, Gubbins KE (1997) A molecular simulation study of freezing/melting phenomena for Lennard-Jones methane in cylindrical nanoscale pores. J Chem Phys 107(22):9659–9667

Maniwa Y, Kataura H, Abe M, Udaka A, Suzuki S, Achiba Y, Kira H, Matsuda K, Kadowaki H, Okabe Y (2005) Ordered water inside carbon nanotubes: formation of pentagonal to octagonal ice-nanotubes. Chem Phys Lett 401(4–6):534–538

Mathivet L, Cribier S, Devaux PF (1996) Shape change and physical properties of giant phospholipid vesicles prepared in the presence of an AC electric field. Biophys J 70(3):1112–1121

Meyer F, Smit B (2009) Effect of cholesterol on the structure of a phospholipid bilayer. Proc Natl Acad Sci USA 106(10):3654–3658

Meyer EE, Rosenberg KJ, Israelachvili J (2006) Recent progress in understanding hydrophobic interactions. Proc Natl Acad Sci USA 103(43):15739–15746

Meyer F, Benjamini A, Rodgers JM, Misteli Y, Smit B (2010) Molecular simulation of DMPC-cholesterol phase diagram. J Phys Chem B 114(32):10451–10461

Nakamura H, Tamura Y (2005) Phase diagram for self-assembly of amphiphilic molecule C12E6 by dissipative particle dynamics simulation. Comput Phys Commun 169(1–3):139–143

Nyström JH, Lönnfors M, Nyholm TKM (2010) Transmembrane peptides influence the affinity of sterols for phospholipid bilayers. Biophys J 99(2):526–533

Özen AS, Sen U, Atilgan C (2006) Complete mapping of the morphologies of some linear and graft fluorinated co-oligomers in an aprotic solvent by dissipative particle dynamics. J Chem Phys 124(6):064905

Powell MR, Cleary L, Davenport M, Shea KJ, Siwy ZS (2011) Electric-field-induced wetting and dewetting in single hydrophobic nanopores. Nat Nanotechnol 6(12):798–802

Rijcken CJ, Snel CJ, Schiffelers RM, van Nostrum CF, Hennink WE (2007) Hydrolysable core-crosslinked thermosensitive polymeric micelles: synthesis, characterisation and in vivo studies. Biomaterials 28(36):5581–5593

Ryjkina E, Kuhn H, Rehage H, Muller F, Peggau J (2002) Molecular dynamic computer simulations of phase behavior of non-ionic surfactants. Angew Chem Int Ed 41(6):983–986

Rzayev J, Hillmyer MA (2005) Nanochannel array plastics with tailored surface chemistry. J Am Chem Soc 127(38):13373–13379

Shapiro RA, Brindley AJ, Martin RW (2010) Thermal stabilization of DMPC/DHPC bicelles by addition of cholesterol sulfate. J Am Chem Soc 132(33):11406–11407

Shikata T, Hirata H, Kotaka T (1987) Micelle formation of detergent molecules in aqueous media. Viscoelastic properties of aqueous cetyltrimethylammonium bromide-salicylic acid solutions. Langmuir 3(6):1081–1086

Shikata T, Hirata H, Kotaka T (1989) Micelle formation of detergent molecules in aqueous media. 3. Viscoelastic properties of aqueous cetyltrimethylammonium bromide-salicylic acid solutions. Langmuir 5(2):398–405

Shillcock JC, Lipowsky R (2002) Equilibrium structure and lateral stress distribution of amphiphilic bilayers from dissipative particle dynamics simulations. J Chem Phys 117(10):5048–5061

Shillcock JC, Lipowsky R (2005) Tension-induced fusion of bilayer membranes and vesicles. Nat Mater 4(3):225–228

Strekalova EG, Mazza MG, Stanley HE, Franzese G (2011) Large decrease of fluctuations for supercooled water in hydrophobic nanoconfinement. Phys Rev Lett 106(14):145701

Yamamoto S, Hyodo S (2005) Mesoscopic simulation of the crossing dynamics at an entanglement point of surfactant threadlike micelles. J Chem Phys 122(20):204907

Yang H, Coombs N, Ozin GA (1997) Morphogenesis of shapes and surface patterns in mesoporous silica. Nature 386(6626):692–695

Yoon DK, Deb R, Chen D, Korblova E, Shao R, Ishikawa K, Rao NVS, Walba DM, Smalyukh II, Clark NA (2010) Organization of the polarization splay modulated smectic liquid crystal phase by topographic confinement. Proc Natl Acad Sci USA 107(50):21311–21315